Materials and Corrosion

Corrosion Resistance of Titanium Dioxide Anodic Coatings on Ti-6Al-4V

SCHOLARONE™
Manuscripts

1
2
3
4
5
6
7
8
9
10
11
12
13
14
15
16
17
18
19
20
21
22
23
24
25
26
27
28
29
30
31
32
33
34
35
36
37
38
39
40
41
42
43
44
45
46
47
48
49
50
51
52
53
54
55
56
57
58
59
60

Corrosion resistance of titanium dioxide anodic coatings on Ti-6Al-4V

M. L. Vera*, E. Linardi, L. Lanzani, C. Mendez, C. E. Schvezov, and A. E. Ares

M. L. Vera, C. Mendez, C. E. Schvezov, A. E. Ares
Instituto de Materiales de Misiones (IMAM), CONICET-UNaM. Félix de Azara 1552 (3300)
Posadas, Misiones, (Argentina)
Facultad de Ciencias Exactas, Químicas y Naturales, Universidad Nacional de Misiones
(UNaM). Félix de Azara 1552 (3300) Posadas, Misiones, (Argentina.)
E-mail: lauravera@fceqyn.unam.edu.ar

E. Linardi, L. Lanzani
Centro Atómico Constituyentes (CAC-CNEA). Av. Gral. Paz 1499 (1650) San Martín,
Buenos Aires, (Argentina)
Instituto Sabato, Universidad Nacional de San Martín, Comisión Nacional de Energía
Atómica. Av. Gral. Paz 1499 (1650) San Martín, Buenos Aires, (Argentina.)

Abstract

The Ti-6Al-4V alloy is used for biomedical implants due to its corrosion resistance and

biocompatibility, associated with the spontaneous formation of TiO_2 oxide. However, the

native film may be flawed and after some time of implantation in the body it may release

metal ions. Oxides of higher thickness than naturally grown can be produced by anodic

oxidation.

The objective of this study was to evaluate the corrosion resistance of anodic TiO_2 coatings,

evaluating the influence of the thickness and crystalline structure of the coatings. Amorphous

coatings were obtained from 27 nm to 140 nm that crystallized in anatase and rutile phases by

heat treatment. The corrosion resistance was evaluated by potentiodynamic measurements in

0.9% sodium chloride which is the main component of physiological solution.

Evaluation of the electrochemical parameters showed that anodic coatings are a more efficient

barrier than the natural TiO_2 oxide.

As the oxidation processes influenced the electrochemical properties of metals by altering the

resistance to corrosion, therefore they become important to study the electrochemical

behaviour of the oxides by electrochemical impedance spectroscopy.

Keywords: corrosion resistance, titanium dioxide coating, Ti-6Al-4V, anodic oxidation.

1.   Introduction

As a means of building a new heart valve design Ti-6Al-4V alloy coated with titanium

dioxide (TiO_2) is selected [1]. TiO_2 coatings have hemocompatibility properties appropriate

for use in this type of prosthesis [2]. In addition to the blood compatibility and wear

resistance, the corrosion resistance in biological fluids is necessary among the requirements

for materials used in cardiovascular devices [3].

Although it is commonly accepted that Ti alloys exhibit high stability and resistance to

corrosion in-vitro due to the formation of a natural oxide, there are several reports showing Ti

accumulation in tissues adjacent to the implant, indicating the release of ions and some degree

of corrosion in-vivo to contact for extended periods of time with the extracellular body fluids,

such as blood and interstitial fluid [4]. As a consequence, it becomes necessary to add thicker

and more protective coatings than the TiO_2 natural oxide.

The anodic oxidation method may produce oxides of uniform thickness on flat and curved

surfaces. The coating thickness can be controlled with the voltage applied between the anode

(sample) and the cathode [5]. From previous studies of our group [6, 7] and other authors [8,

9] it is known that when a Ti-6A1-4V alloy is anodically oxidized, employing 1 M sulphuric

acid as the electrolyte at voltages as high as 60 V, coatings are homogeneous and amorphous.

As hemocompatibility of TiO_2 is also determined by the surface roughness, and crystal

structure of the oxide [10], it is necessary to perform a heat treatment to coated samples to

obtain crystalline coatings. It was found that, for 1 h at 500 °C crystalline coatings were

obtained without significantly changing the thickness and morphology of them [11].

As previously mentioned, one of the properties of the coatings for use in cardiovascular devices to be evaluated is the corrosion resistance in biological fluids, in which the sodium chloride is one of the main components [12, 13]. Blood plasma contains sufficient chloride concentration to corrode metal materials, so it is necessary to evaluate this property in that environment [14]. *Schaldach et al*.[13] propose that a good way to evaluate the extent to which a material is affected by the contact with the blood is measuring the corrosion electrochemically by means of polarization curves.

In blood plasma, the sodium chloride is at a concentration of 0.9%, so that a physiological solution of 0.9% sodium chloride was used to evaluate the corrosion resistance by polarization curves in this medium. The pH in the solution was maintained at 5.5 by considering the worst case associated with inflammatory processes in the body, during which the normal pH of the body (pH = 7) may decrease to such values, causing potential gradients and current density and thus enabling acceleration of the corrosion processes [15].

In this work we present and analyze comparatively the polarization curves in 0.9% sodium chloride substrate with and without anodic coating and after these with and without heat treatments. Furthermore, for the presence of chlorides in the medium it was also necessary to determine whether localized pitting corrosion occurs, for which a reverse polarization was made [16].

Thermal and anodic oxidation are surface modification processes that have a significant effect on the electrochemical properties of metals and alloys, which may alter the corrosion resistance of the materials to be used as implants, therefore it becomes important to study the electrochemical behavior of the oxides formed. Comparisons of the electrochemical parameters between the uncoated substrate coatings allow identifying the need of manufacturing the last ones [17].

Studying the behavior of the coatings by electrochemical impedance spectroscopy (EIS) depends on the electrolyte used in the study, since there are various types of surface alterations induced by the medium, such as adsorption of species, coarsening, dissolution, etc. Results of EIS are presented and discussed comparatively between bare substrate and coatings in different media: in 1 M sulphuric acid, which is the medium of growth of anodic coatings, and in 0.9% sodium chloride simulating the environment at which it will be exposed in service.

There is a large amount of experimental data available in the literature both polarization tests in biological media as well as EIS in different media. So, the close relationship between the growth conditions of surface films and their structural characteristics as well as their corrosion resistance make it necessary to study the behaviour of anodic films, allowing their future comparison to *in-vitro* and *in-vivo* tests.

2.   Experimental

2.1. Surface preparation of the substrate

Plates of (1 x 2) cm^2 and 0.2 cm thick of Ti-6Al-4V alloys were used as a substrate for oxidations. These were roughly shaped with SiC abrasive papers of increasing granulometry from #120 to #1500 and polished, first with diamond paste 1 μm lubricated with ethylene glycol and then with 4:1 colloidal silica and hydrogen peroxide mixture, to obtain a specular surface. Subsequently, the samples were cleaned with water and detergent, then wiped with alcohol and dried with hot air. Substrate sample was identified as TiG5.

2.2. Anodic oxidation

The anodic oxidation was done at room temperature, circulating direct current between the

anode of Ti-6Al-4V and a cathode of Pt, spaced 5 cm apart, submerged in 1 M sulphuric acid

electrolyte solution. The oxidation process was carried out at constant voltage for 1 minute. A

different voltage in each sample was used, from 10 V to 100 V (see Table 1). Immediately

after the oxidation, the samples were rinsed with deionized water and dried with hot air.

2.3. Heat treatments

Anodic coatings of 20 V, 40 V and 60 V were thermal treated at 500 °C for 1 h. A heating

rate of 10 ° C / min was used. The cooling was slow inside the furnace.

Additionally, the same treatment was carried out at 500 °C to a substrate of Ti-6Al-4V

(without anodic oxidation) to compare the effect of the thermal oxidation. This sample was

identified as Ai-T500-t1.

The nomenclature used for each sample is presented in Table 1. The conditions under which

they were obtained and the thickness and crystalline structure of each, which were previously

determined by X-ray reflectometry and X-ray diffraction, respectively, were published in

previous works of *Vera et al.* [11, 18, 19].

For analysis of the results, the coatings were grouped in Table 1 according to the oxidation

process used in: Group A (anodic coatings in pre-spark and post-spark conditions), Group T

(thermal coatings) and AT500 Group (anodic coatings followed by heat treatment at 500 °C).

2.4. Evaluation of corrosion resistance

To evaluate the electrochemical behavior of the substrate and coatings a potentiodynamic

polarization was performed. A Gamry Series G, PC4-750 equipment and a cell of three

electrodes were used: sample, a Pt wire counter electrode and a reference electrode. Aerated

solutions were used as electrolytes: 0.9% sodium chloride (30 ºC, pH = 5.5), in which case a

reference electrode of saturated calomel [Hg, Hg_2Cl_2/KCl (satured solution)] was used; and 1

M sulphuric acid (pH = 1.13) with a mercury / mercurous sulphate electrode, [Hg,

$HgSO_4$/K_2SO_4 (saturated solution)].

To observe the surfaces before and after corrosion testing, a metallographic optical

microscope and a scanning electron microscope (SEM) were used.

2.4.1. Polarization curves

After one hour at open circuit at corrosion potential (E_{corr}) of each sample in each electrolyte,

potentiodynamic measurements were performed from -0.02 V to 1.5 V with respect to E_{corr},

with a scan rate of 0.2 mV / s.

To evaluate if there was pitting, a cyclic polarization scan was performed between the same

values mentioned above and with the same potential sweep rate of 0.2 mV/s in both

directions.

2.4.2. Electrochemical impedance spectroscopy (EIS)

Electrochemical impedance measurements were performed using a signal with amplitude of ±

5 mV and a frequency range between 0.001 Hz and 60.000 Hz, with 10 points per decade. We

worked with two types of electrolytes:

- 1 M sulphuric acid (at E_{corr} and E_{pas}) with sulfate reference electrode, to determine the

   characteristics in the medium in which the films grow.

- 0.9% sodium chloride (at E_{corr}) with calomel reference electrode (SCE), to evaluate

the performance of the films in the media for which they were prepared.

The EIS results were fitted by least squares models to equivalent circuits using a calculation

program. As different equivalent circuits can lead to a good fit of a set of experimental results

for the selection of an equivalent circuit representing the experimental behavior of the system,

the following criteria were used: adjustment of the proposed circuit with the experimental

results with a certain value of error (in this work, $\chi^2 < 1.10^{-3}$); values of circuit parameters

related to the structure or electronic behavior of the system [20].

3.   Results and discussion

3.1. Polarization curves

Polarization curves of TiG5 sample and coated samples, whose properties are summarized in

Table 1 are presented in Figure 1. We can clearly see the difference between the value of E_{corr}

of uncoated TiG5 sample (- 263 mV_{SCE}) and the values of E_{corr} of the samples with coating

displaced towards positive values (noble) of potential, ranging from 37 to 198 $mV_{SCE.}$

According to *Vetter*, displacement of E_{corr} values is linked to compositional and structural

changes of the surface film [21].

It is observed in Figure 1 that the polarization curve of TiG5 sample has some irregularities

for increasing i, immediately after E_{corr}, that could correspond to the dissolution of vanadium

according to the *Pourbaix* diagram, correlating to this element in the test conditions [22]. In

this regard, *Hukovic et al.*[23] reported that V was dissolved in vanadyl ions (VO^{2+}) in

physiological solution causing the current to increase at 0 V_{SCE}, while the Al pitting corrosion

can occur at -0,5 V_{SCE}. This would justify the necessity of coating on the alloy [24, 25],

whereas ions can eventually migrate to tissues where the device is implanted.

Electrochemical parameters extracted from the curves of Figure 1 corresponding to each

sample are summarized in Table 2.

E_{pas} is the potential at which passivity starts. In Table 2, E_{pas}-E_{corr} value indicates the area of

increasing i up to the passive zone in which i is stabilized at a constant value. The substrate

TiG5 has an increasing zone of i of 763 mV from E_{corr} to achieve passivity at 500 mV. In

contrast, in the coated samples E_{pas}-E_{corr} is 0 mV (Table 2) because they are passive because

of the presence of the coating. Figure 1 and Table 2 show that in all the samples analyzed,

current densities in the range of the potentials measured are less than 1 $\mu A/cm^2$. The values of

current densities in the passive zone of coated samples using voltages from 10 to 70 V is three

orders of magnitude lower (i_{pas} = 4 to 10 nA/cm^2) than that corresponding to the uncoated

TiG5 sample (880 nA/cm^2). These values of i_{pas} corresponding to coated samples were even

lower than those reported by other authors who tested TiO_2 coatings synthesized by different

techniques and using the same electrolyte [8, 26].

S1-V100 sample (Group A post-spark) curve has the highest i_{pas} value (105 nA/cm^2) among

the anodized samples, which could be related to its greater thickness and crystal structure of

anatase and rutile (see Table 1) and also to the presence of pores on the surface. This may be

due to an increase of the conductivity in the anodized potential which produced a soften effect

of the barrier film as compared to the one achieved with the compact coatings obtained at

lower voltages than the spark formation, where there was a greater resistance to the current

flow [26, 27].

The S1-V70 sample, also belonging to Group A post-spark, has been obtained to limit voltage

spark, and it is crystalline in anatase phase as shown in Table 1. However, it has a similar

performance against corrosion than samples from Group A pre-spark, i.e., the level of

roughness, porosity and crystallinity that does not affect their performance against corrosion

in the medium of study.

E_{trans} value is the value that indicates the potential onset of transpassivity. In Table 2, the

E_{trans}-E_{pas} value indicates the range in potentials in which the current was kept constant. In the

TiG5 substrate, in the range of measured potentials, there is no increase in the current, that is,

no transpassivity occurs. However, all other coated samples except the S1-V100 sample,

showed a gradual increase in i that began between 620 and 960 mV_{SCE}, indicating the start of

a zone of transpassivity. That increasing in i by transpassivity is not observed in the curve of

S1-V100 sample in Figure 1, and could be due to its greater thickness (see Table 1).

Taking into account the i increases previously mentioned and considering that Cl$^-$ is an

aggressive anion that can produce pitting in titanium alloys [16], a cyclic polarization was

carried out using a sample with anodic coating (S1-V40) to evaluate that the possibility of the

i increase is due to pitting corrosion.

In Figure 2 it can be seen that there is no pitting because the hysteresis curve in its reverse

path of potential is not present [28, 29]. This result agrees with the fact that no evidence of

pitting in the coatings using optical microscope and SEM after performing polarization tests

has been observed (Figure 3). In this regard, it is worth mentioning that the trials did not

change the colour of the coatings, indicating that the thickness did not change [30].

In Figure 2 the value of 600 mV_{SCE}, where i increase starts, coincides with the value of the

oxygen evolution potential, by decomposition of water, at pH 5.5 [22]. This suggests that the

coating corresponds to a conductive oxide [16]. Several authors showed the same increases in

i curves for similar coatings, some did not justify [26, 27] and others, attributed the increase

to the current course of the reaction of oxygen [28, 31, 32].

The i_{corr} calculated from the slopes of Tafel [16] for TiG5 sample was 0.8 nA/cm^2, a value

which agrees with that found by *Pouranvari* and *Bidhendi* [28] in Hank's solution. From the

value of i_{corr} a corrosion rate of 7 nm/year was measured. According to this value, by

generalized corrosion, the thinnest part of the valve, of 1 mm (located in the region of pivot

for opening and closing the valves [33]) would have a useful life of 14,400 years.

However, considering the geometry and operating mechanism of the device [34] other types

of corrosion may occur, like crevice corrosion or phenomena associated to the erosion-

corrosion of the material. This study is proposed as future work to the present research. These

mechanisms could significantly accelerate the degradation process, that is why it is necessary

to coat the piece, because as it has been seen the coating further improves the electrochemical

parameters. In this sense, the highlight is the low value of i_{pas} of the coatings.

Polarization curves of samples anodized to 20 V, 40 V and 60 V with and without heat

treatments for 1 h at 500 °C, corresponding to Groups A and AT500, and whose thicknesses

and structures are described in Table 1, are shown in Figure 4. The curves corresponding to

the TiG5 sample and coatings obtained by thermal oxidation, Ai-T500-t1 (Group T) are

included in Figure 4.

Regarding the shape of the polarization curves with and without heat treatment, in Figure 4 it

can be seen that the curves of the samples of AT500 Group are a combination of the curves

corresponding to those in Group A (pre-spark) and the sample of Group T. E_{corr} values of the

samples with heat treatment approaching the uncoated substrate, while the anodized samples

of Group A showed nobler E_{corr} values. Similarly i_{pas} values are higher for the samples with

heat treatment compared to those without it. This may be because the heat treated samples

exhibit crystalline coatings, as summarized in Table 1, and the crystallinity of an oxide

implies the presence of defects such as grain boundaries, dislocations, stacking faults, second

phases, etc., which can deteriorate the corrosion resistance of the film [35]. In this regard,

Diamanti et al.[26] demonstrated by EIS studies that the presence of crystalline phases in the

oxide surface offers less resistance to the charge transfer of surfaces completely amorphous.

Regarding transpassivity, it should be mentioned that in both groups of samples, it is given

that i increased at the potential for oxygen evolution (between 600 and 900 mV$_{SCE}$) [16, 22]

and then stabilizes at a higher value of i.

3.2. Electrochemical impedance spectroscopy (EIS)

3.2.1.   Electrochemical impedance spectroscopy in 1 M sulphuric acid

For construction of cardiovascular devices homogeneous and low surface roughness are

required, such as anodic oxidation coatings obtained at lower voltages than 70 V [18], being

these materials which have lower passive current densities relative to other. That is why the

characterization by EIS in 1 M sulphuric acid was performed on TiG5, S1-V20 and S1-V40

samples.

Polarization curves of TiG5, S1-V20 and S1-V40 samples made in 1 M sulphuric acid are

presented in Figure 5. 1 M sulphuric acid is the medium used as an electrolyte in the anodic

oxidation to grow the coatings. In this figure, the corrosion potential of the three samples and

the potential (0.6 V$_{SCE}$) to which EIS tests were performed, are observed. As it was observed

in the polarization curves performed in 0.9% sodium chloride, substrate (TiG5) has a region

of increased current density from the corrosion potential (-0.328 V$_{SCE}$) until it is stabilized

with a current density of passivity around 2 μA, while the coated samples are passive from the

corrosion potential (located at approximately 0.2 V$_{SCE}$, more noble than the TiG5 value) with

passive current densities less than two orders of magnitude (~ 10 nA).

The results of the EIS tests in 1 M sulphuric acid are shown in Figure 6. It made at corrosion

potential E$_{corr}$ (Figure 6 (a)) and a potential of passivity (Figure 6 (b)). In both figures the

small dotted lines correspond to the results of the equivalent circuits corresponding to that

described below in each case setting.

In Figure 6 (a), in the Bode graph showing TiG5 unanodized sample (at E_{corr}), two zones are observed: a high frequency range, where both the impedance module as the angle are closer to 0 and, another zone, in a range of medium and low frequency (between 0.01 and 100 Hz), having a modulus of impedance with a slope close to 1 and the phase angle close to -90 °. The first zone is related to the strength of the solution and the latter is characteristic of the capacitive behavior of the titanium oxide films formed in air [26, 36].

Furthermore, in Figure 6 (b) in the Bode graph showing unanodized TiG5 sample (at E_{pas}), three zones are observed: areas of high and medium frequency are similar to those previously described in Figure 6 (a) (at E_{corr}). However, at low frequencies there is another area where the plateau of constant phase angle was removed. The latter area could be related to the resistance of the film formed by the polarization at low potentials, which probably reduced stability [26].

In the Bode diagrams corresponding to the anodised samples in Figure 6 (a) and (b), it can be seen that anodizing decreases the phase angle for material unanodized and a shift in the phase angle region is observed nearly constant to higher frequencies. An increase of impedance of about one order of magnitude, with respect to the unanodized material is also observed. Both effects induce the appearance of a second time constant in impedance and are related to an increase in thickness of the passivating film of anodized product, accounting for the bulk resistivity of the anodic film, thicker than the native, which correlates with lower i_{pas} observed in Figure 5 [37].

EIS results of unanodized substrate, TiG5, both at E_{pas} and E_{corr}, can be described using the Randles circuit (Figure 7), where R_{sol} is the resistance of electrolyte, and R_1 and Q_1 in parallel representing the resistance and capacitance of the passive film.

Due to the low thickness of the native film formed on the titanium unanodized (1.5 to 10 nm), some authors consider it as included in the capacity of the double layer [26]. Constant phase

element (CPE) was used to represent the elements of pseudocapacitance (Q) instead of pure

capacitors (C) to consider possible deviations from ideality in the capacitive response

systems. This impedance element is defined by the following equation (1) [38]:

$$Z_{CPE} = [Q(2\pi fi)^n]^{-1} \tag{1}$$

Where $-1 \leq n \leq 1$ relates to a non-uniform current due to inhomogeneities of the films or

surface roughness distribution. When $n=1$ the behavior is that of an ideal capacitor.

As noted in Figure 6 (a) and (b), the EIS anodic films exhibit more complex than for the

substrate TiG5 response, two regions characterized by different time constants, that are

associated with a complex structure which can be described using a two-layer model, in which

the inner layer results dominate impedance at higher frequencies, while a porous outer layer

dominates the impedance curves at low frequencies [26, 37]. In the literature different

equivalent circuits for reproducing the results of anodic films of bilayer structures have been

proposed, using different configurations of R / C or CPE pairs in parallel, associated in series

or in parallel with or without cascade [26, 30, 37, 39-42]. From results of EIS analysis of S1-

V20 and S1-V40 anodic coatings the best fit of experimental results were obtained ($\chi^2 < 1.10^{-3}$)

and according to the characteristics of the coatings with the circuitry described below. EIS

results of Figure 6 of S1-V20 film at E_{corr} and E_{pas} is tightened with the circuit of Figure 8. In

this circuit Q_1 corresponds to a pseudocapacitance of the thickest layer, whereas Q_2 with

values of n_2 equal to 0.56 is related to a pseudocapacitance due to the dispersion of frequency

in the pores and is used to represent the processes that occur at inner pores [37, 43]. This

configuration has been used by *Gomez Sanchez et al.* [37] to describe zirconium anodic

coatings obtained up to 12 V and anodic titanium coatings up to 30 V.

EIS results of S1-V40 film at E_{corr} and E_{pas} of Figure 6 were adjusted with the circuit of Figure

9. The basic assumption of this circuital description lies in the presence of a bilayer with defects in the outer and the inner layer, which causes a non-ideal capacitive behaviour in both layers, which together give rise to the charge transfer to throughout the coating, allowing the transport along the metal/oxide/electrolyte system [37].

Comparing circuits proposed to describe the results of EIS for S1-V20 and S1-V40 shows that the resistive component (R_2) was added. According to Table 4 the value of $n_1 = 0.88$ of S1-V40 coating at E_{corr} indicates that this layer would be less dense and / or with major defects with respect to the corresponding S1-V20 ($n_1 = 0.95$). The values also indicated that this layer would present greater capacity (Q_1) and a resistor (R_1) negligible, the latter associated with the resistance in the pores. The evolution of the bilayer system with increased anodizing voltage associated with the characteristics of such coatings were acquired at different voltage ranges.

The circuit of Figure 9 was described by *Orazem* and *Tribollet* [38], who suggest that the substrate-oxide system behaves as an electrode partially blocked by a coating which does not cover the entire surface of the metal, but has a certain "degree of coverage" of the characteristic conditions of film growth and it confers protection to isolated zones along the same areas (Figure 10). This description of the structure is consistent with the growth morphology of the anodic film which is dependent on the structure and crystal orientation of the material used as a substrate, indicating that it is not completely uniform over the entire surface of the metal [18]. Also, depending on the voltage at which the anodizing is done, micropores product of increasing electric field begin to form and the evolution of oxygen through the film, leading to the breakdown and then to spark with increasing anodizing voltage [18].

According to Figure 10, in the interface located at the end of the pore, the impedance results in a combination in parallel mode. Inside the pore the resistance is R_1 and the insulating

coating can be considered as a pseudocapacitor Q_1, that is in parallel with the impedance of the pore [38].

This arrangement of two cascaded CPE, which accounted for a layer with higher density and insulating (Q_1 and R_1) and more porous (Q_2 and R_2) has been used by other authors to describe the behavior of anodic films on zirconium oxidized at 24 V and titanium at 30 V [30, 37].

3.2.2. Electrochemical impedance spectroscopy in 0.9% sodium chloride

In Figure 11 EIS results performed in 0.9% sodium chloride of the TiG5 and S1-V40 samples at the corrosion potential are shwon. The continuous lines and small dots correspond to the results of the equivalent circuits corresponding to that described below in each case setting. In Figure 11 an increase in the impedance modulus of the system between the anodized and unanodized samples, and an offset phase angle in the higher frequencies to superior frequencies can be seen. This can be related to an increase in the oxides thickness anodizing, which is in agreement with the decrease in the current density observed in the anodic polarization curves due to an increase of the barrier effect (Section 3.1).

The results of EIS in 0.9% sodium chloride for unanodized TiG5 can be described by the Randles circuit of Figure 12, which depicts a protective dense oxide film that acts as a barrier between the environment and the metal. Different authors used to describe this circuit behavior without anodizing titanium in various solutions that imitate biological fluid [23, 44, 46].

The EIS results of S1-V40 anodic coating in 0.9% sodium chloride can be described by the equivalent circuit of Figure 13.

This circuit pattern can be explained by considering the two porous layers proposed by

Orazem and *Tribollet* [38], who consider that in a system exposed to a corrosive environment, a thin layer of salt can be deposited on the electrode. In this case it was covered with an oxide and could be previously described according to the circuit shown in Figure 8, so that the superposed two layers can be connected in an additional series circuit further considering the effect of the new outer porous layer (with $n_1 \approx 0.7$), as shown in Figure 14. The settings of the model are presented in Table 5.

In the circuit of Figure 13 and Figure 14, R_2 and Q_2 correspond to the resistance and pseudocapacity of oxide coating layer, with $n_2 \approx 0.8$. On the other hand, Q_3, with $n_3 \approx 0.5$, represents diffusion processes within the pores [47, 48].

Aziz-Kerrzo et al. [47] use the same circuit of Figure 14 to raise the formation of two layers to describe the behavior of Ti cp after various immersion times in phosphate buffer. However, non-porous outer layer were formed over Ti cp exposed to 0.9% sodium chloride, indicating that the formation of the second porous layer in the early stages of immersion is dependent on the nature of the electrolyte and the ions present therein, as well as the surface characteristics of the electrodes.

As noted, the circuit models used to describe the results of EIS in 0.9% sodium chloride differ from those proposed for the anodic films in the anodizing solution (1 M sulphuric acid). This is because the EIS technique is sensitive to changes on the surface as a result of the interaction between the material and the electrolyte used.

4.   Conclusions

Through polarization curves in saline solution (0.9% sodium chloride), the corrosion resistance of the TiG5 substrate and coatings made by anodic oxidation with 1 M sulphuric acid at different voltages (from 10 to 100 V) with and without subsequent heat treatment (1 h

at 500 °C) were evaluated.

The evaluation of the extracted electrochemical parameters of polarization curves demonstrated that anodic coatings are more efficient than the oxide layer spontaneously formed on the bare substrate (TiG5). E_{corr} values of the coatings were nobler than the substrate E_{corr} value, the oxide layer passivates the surface and passive current densities were three orders lower in magnitude than the corresponding substrate. Moreover the coatings showed no evidence of localized corrosion by pitting.

For the coatings obtained with voltages of 10-70 V (27 nm to 170 nm respectively) no clear trend of increasing or decreasing the current of passivity with the thickness of the coatings was found, and it was between 4 and 10 nA/cm^2.

However, the coating obtained at 100 V (about 240 nm), showed a higher value of i_{pas} as a result of porosity and crystallinity, but lower than that of the bare substrate.

With the thermal treatments carried out on previously anodized samples, electrochemical parameters of polarization curves corresponding to the samples only anodized were changed. E_{corr} values were similar to those of the bare substrate and current densities were higher than for anodized samples, indicating that the crystallinity deteriorates the corrosion resistance of the coatings. The current densities are lower than that of the bare substrate.

As the release of ions, although minimal, can cause problems in the body, it is concluded that TiO_2 coatings are required, as they have been shown to significantly improve the performance of the material in the medium of the study.

The most favourable coatings would be obtained by anodic oxidation at low voltages, without heat treatment, by homogeneity and excellent polarization results in biological fluids.

Moreover, by means of the electrochemical impedance spectroscopy (EIS) we analysed the structural characteristics of the bare substrate and anodic films through adjustment of the results with different circuit models, which were related to the results obtained during surface

characterization of materials. EIS behavior of anodic films on Ti-6Al-4V in anodizing

medium (1 M sulphuric acid) was associated with a structure composed of two layers, a dense

layer and a porous one, which configuration changed with the potential of anodization. This

was consistent with the changes observed for the growth of these coatings.

Moreover, the response of the anodic films in 0.9% sodium chloride was consistent with a

circuit model of two layers, involving the interaction with the immersion medium.

5   References

[1] O. N. Amerio, M. R. Rosenberger, P. C. Favilla, M. A. Alterach, C. E. Schvezov, *Rev. Arg. Cir. Card.* **2006**, *4,* 70.
[2] N. Huang, P. Yang, Y. X. Leng, J. Y. Chen, H. Sun, J. Wang, G. J. Wang, P. D. Ding, T. F. Xi, Y. Leng, *Biomater.* **2003**, *24,* 2177.
[3] Y. X. Leng, N. Huang, P. Yang, J. Y. Chen, H. Sun, J. Wang, G. J. Wan, X. B. Tian, R. K. Y. Fu, L. P. Wang, P. K. Chu, *Surf. Coat. Tech.* **2002**, *156,* 295.
[4] M. Long, H. J. Rack, *Biomater.* **1998**, *19,* 1621.
[5] A. Aladjem, *J. Mater. Sci.* **1973**, *8,* 688.
[6] M. L. Vera, A. E. Ares, D. Lamas, C. E. Schvezov, *Anales AFA* **2008**, *20,* 178.
[7] M. L. Vera, A. E. Ares, M. R. Rosenberger, D. G. Lamas, C. E. Schvezov, *Anales AFA* **2009**, *21,* 174.
[8] D. Velten, V. Biehl, F. Aubertin, B. Valeske, W. Possart, J. Breme, *J. Biomed. Mater. Res.* **2002**, *59,* 18.
[9] M. V. Diamanti, M. P. Pedeferri, *Corros. Sci.* **2007**, *49,* 939.

[10] C. E. Schvezov, M. A. Alterach, M. L. Vera, M. R. Rosenberger, A. E. Ares, *JOM* **2010**, *62,* 84.

[11] M. L. Vera, M. R. Rosenberger, D. G. Lamas, C. E. Schvezov, A. E. Ares, *Actas IBEROMET XII y X CONAMET/SAM* **2010**, T2-143.

[12] C. Leyens, M. Peters, *Titanium and Titanium Alloys,* Wiley-VCH, Weinheim, **2004**.

[13] M. Schaldach, *Electroterapia del Corazón, Aspectos técnicos en estimulación cardiaca,* Color Press, Walla Walla, Washington, **1993**.

[14] X. Liu, P.K. Chu, C. Ding, *Mater. Sci. Eng. R.* **2004**, *47,* 49.

[15] M. E. P. Souza, L. Lima, C. R. P. Lima, C. A. C. Zavaglia, C. M. A. Freire, *J. Mater. Sci. Mater. Med.* **2009**, *20,* 549.

[16] J. R. Galvele, G. S. Duffó, *Desgradación de Materiales – Corrosión,* Jorge Bauino Ediciones: Instituto Sabato, Buenos Aires, **2006**.

[17] R. Ion, C. Vasilescu, P. Drob, E. Vasilescu, A. Cimpean, S. I. Drob, D. M. Gordin, T. Gloriant, *Mater. Corros.* **2014**, *65,* 593.

[18] M. L. Vera, *Ph.D. Thesis*, Universidad Nacional de General San Martín, Comisión Nacional de Energía Atómica, Instituto de Tecnología "Prof. Jorge A. Sabato", Buenos Aires, **2013**.

[19] M. L. Vera, M. A. Alterach, M. R. Rosenberger, D. G. Lamas, C. E. Schvezov, A. E. Ares, *Nanomater. Nanotechnol.* **2014**, *4,* 1.

[20] N. T. C. Oliveira, S. R. Biaggio, S. Piazza, C. Sunseri, F. Di Cuarto, *Electrochim. Acta*, **2004**, *49,* 4563.

[21] K. J. Vetter, *Electrochemcial Kinetics: Theoretical and Experimental Aspects,* Academic Press, New York, **1967**.

[22] M. Pourbaix, *Atlas of Electrochemical Equilibria in Aquous Solutios*, NACE Cebelcor, Houston, **1974**.

[23] M. Metikos-Hukovic, A. Kwokal, J. Piljac, *Biomater.* **2003**, *24,* 3765.

[24] C. E. B. Marino, S. R. Biaggio, R. C. Rocha-Filho, N. Bocchi, *Electrochim. Acta* **2006**, *51,* 6580.

[25] S. Tamilselvi, V. Raman, N. Rajendran, *Electrochim. Acta* **2006**, *52,* 839.

[26] M. V. Diamanti, F. Bolzoni, M. Ormellese, E. A. Pérez-Rosales, M. P. Pedeferri, *Corros. Eng., Sci. Tech.*, **2010**, *45,* 428.

[27] A. Cigada, M. Cabrini, P. Pedeferri, *J. Mater. Sci.: Mater. Med.* **1992**, *3,* 408.

[28] H. R. A. Bidhendi, M. Pouranvari, *Metalurgija-MJoM*, **2011,** *17,* 13.

[29] P. Shi, F. T. Cheng, H. C. Man, *Mater. Lett.* **2007**, *61,* 2385.

[30] S. A. Fadl-allah, Q. Mohsen, *Appl. Surf. Sci.*, **2010**, *256,* 5849.

[31] K. Y. Chiu, M. H. Wong, F. T. Cheng, H. C. Man, *Appl. Surf. Sci.* **2007,** *253,* 6762.

[32] H-J. Song, M-K. Kim, G-C. Jung, M-S. Vang, Y-J. Park; *Surf. Coat. Tech.* **2007,** *201,* 8738.

[33] M. R. Rosenberger, O. Amerio, C. Schvezov,. *Forth International Congress of Cardiology on the Internet;* CETIFAC–Bioingeniería UNER **2005**. Available: http://www.fac.org.ar/ccvc/llave/tl211/tl211.php

[34] M. R. Rosenberger, O. N. Amerio, C. E. Schvezov, *Mecánica Computacional* **2005**, *XXIV,* 1943.

[35] N. Sato, *Corros. Sci.* **1990,** *31,* 1.

[36] D.J. Blackwood, *Electrochim. Acta* **2000**, *46,* 563.

[37] A. Gomez Sanchez, *Ph.D. Thesis*, Universidad Nacional de General San Martín, Comisión Nacional de Energía Atómica, Instituto de Tecnología "Prof. Jorge A. Sabato", **2011**.

[38] M. E. Orazem, B. Tribollet, *Electroquemical Impedance Spectroscopy*, John Wiley & Sons, Hoboken, New Jersey, **2008**.

[39] V. A. Alves, R. Q. Reis, I. C. B. Santos, D. G. Souza, T. F. Gonçalves, M. A. Pereira-da-Silva, A. Rossi, L. A. da Silva, *Corros. Sci.* **2009**, *51,* 2473.

[40] C. Jaeggi, P. Kern, J. Michler, T. Zehnder, H. Siegenthaler, *Surf. Coat. Tech.* **2005**, *200,* 1913.

[41] T. Shibata, Y.-C. Zhu, *Corros. Sci.* **1995,** *37*, 133.

[42] J. Marsh, D. Gorse, *Electrochim. Acta* **1998**, *43*, 659.

[43] I. Milosev, T. Kosec, H.-H. Strehblow, *Electrochim. Acta* **2008**, *53,* 3547.

[44] J. E. G. González, J. C. Mirza-Rosca, *J. Electroanal. Chem*. **1999,** *471,* 109.

[45] D. Krupa, J. Baszkiewicz, J. W. Sobczak, A. Bilinski, A. Barcz, *J. Mater. Proces. Tech.* **2003**, *143-144*, 158.

[46] M. E. P. Souza, L. Lima, C. R. P. Lima, C. A. C. Zavaglia, C. M. A. Freire, *J. Mater. Sci.: Mater. Med.* **2009**, *20,* 549.

[47] M. Aziz-Kerrzo, K. G. Conroy, A. M. Fenelon, S. T. Farrell, C. B. Breslin, *Biomater.* **2001**, *22,* 1531.

[48] M. Metikos-Hukovic, E. Tkalcec, A. Kwokal, J. Piljac, *Surf. Coat. Tech*. **2003,** *165,* 40.

1
2
3
4
5
6
7
8
9
10
11
12
13
14
15
16
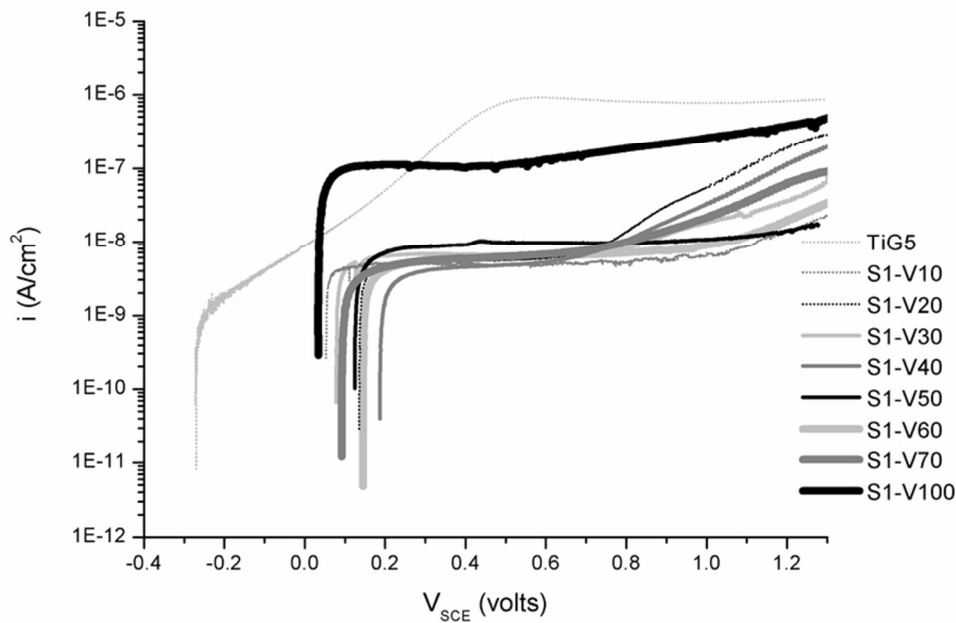17
18
19
20
21
22
23
24
25
26
27
28
29
30

Figure 1. Potentiodynamic polarization curves in 0.9% sodium chloride, of substrate (TiG5) sample and anodized samples with 1 M sulphuric acid, using 10 V to 100 V.
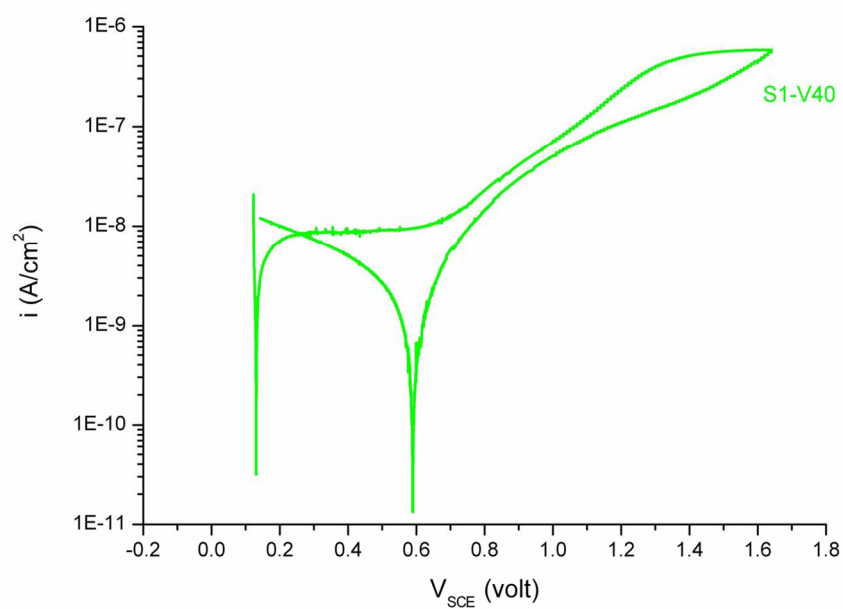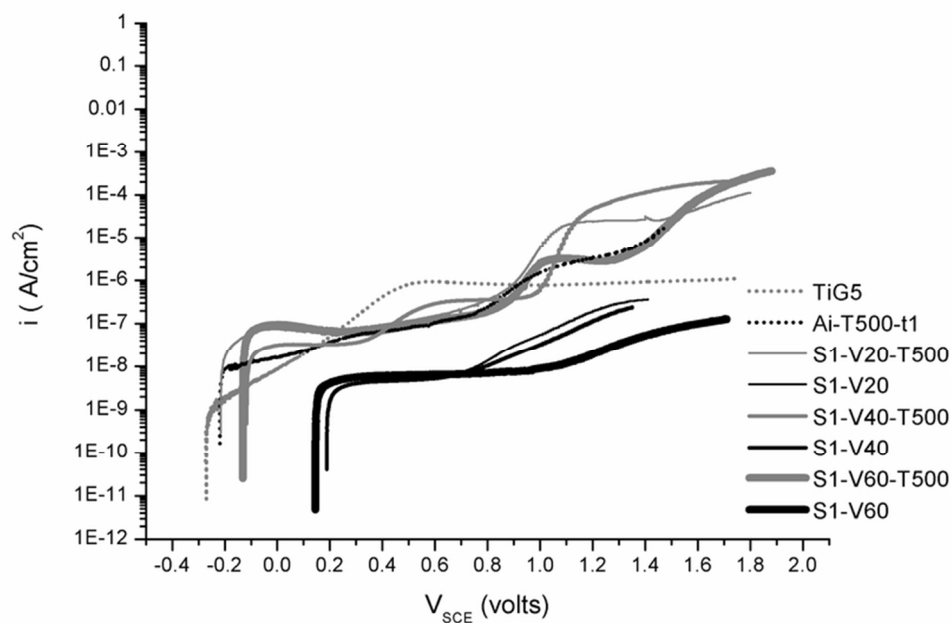71x51mm (300 x 300 DPI)

31
32
33
34
35
36
37
38
39
40
41
42
43
44
45
46
47
48
49
50
51
52
53
54
55
56
57
58
59
60

Figure 2. Cyclic polarization curve in 0.9% sodium chloride of S1-V40 sample.

1
2
3
4
5
6
7
8
9
10
11
12
13
14
15
16
17
18
19
20
21
22
23
24
25
26
27
28
29
30
31
32
33
34
35
36
37
38
39
40
41
42
43
44
45
46
47
48
49
50
51
52
53
54
55
56
57
58
59
60
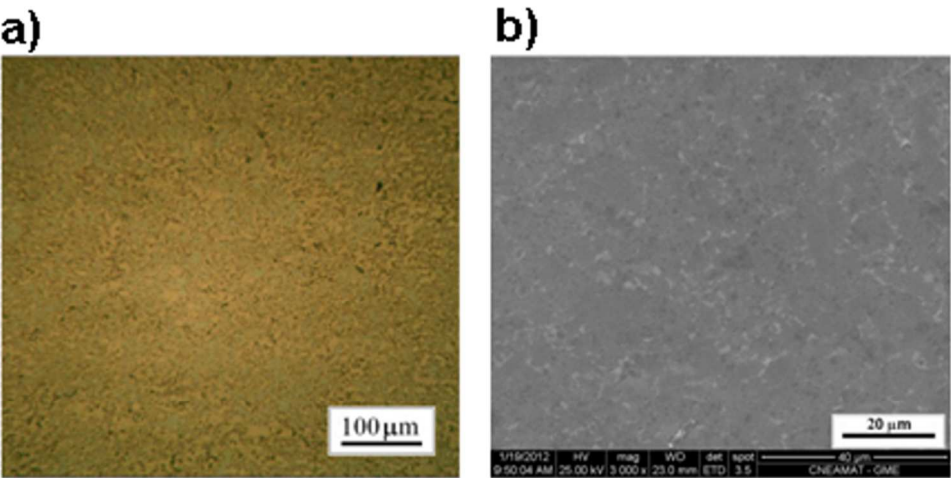
Figure 3. Micrographs after corrosion test in 0.9% sodium chloride of S1-V50 sample: a) optical microscope; b) SEM.

Figure 4. Potentiodynamic polarization curves in 0.9% sodium chloride, of substrate (TiG5) sample and anodized samples without and with heat treatment of 1 h at 500 °C.
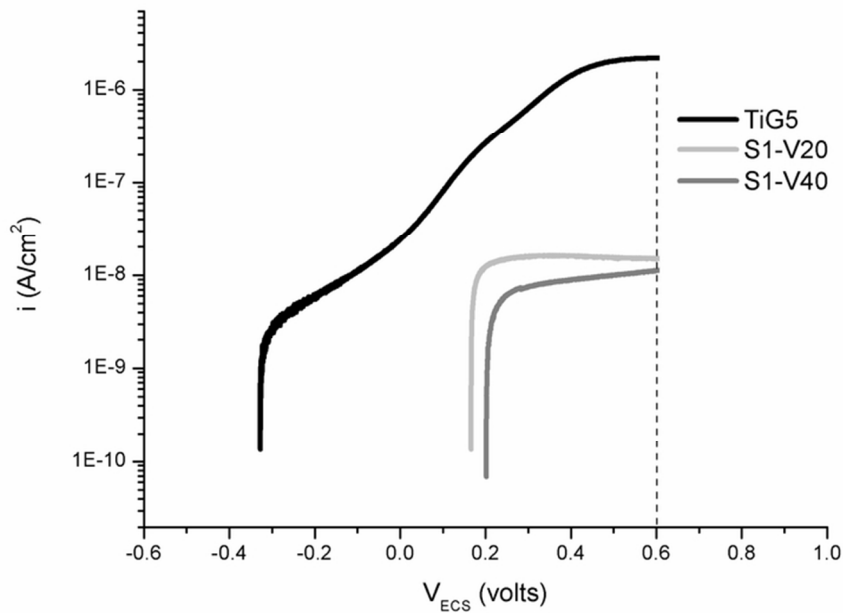71x51mm (300 x 300 DPI)

1
2
3
4
5
6
7
8
9
10
11
12
13
14
15
16
17
18
19
20
21
22
23
24
25
26
27
28
29
30
31
32
33
34
35
36
37
38
39
40
41
42
43
44
45
46
47
48
49
50
51
52
53
54
55
56
57
58
59
60

Figure 5. Polarization curves in 1 M sulphuric acid, of substrate (TiG5) sample and anodized samples (S1-V20 and S1-v40).
71x51mm (300 x 300 DPI)
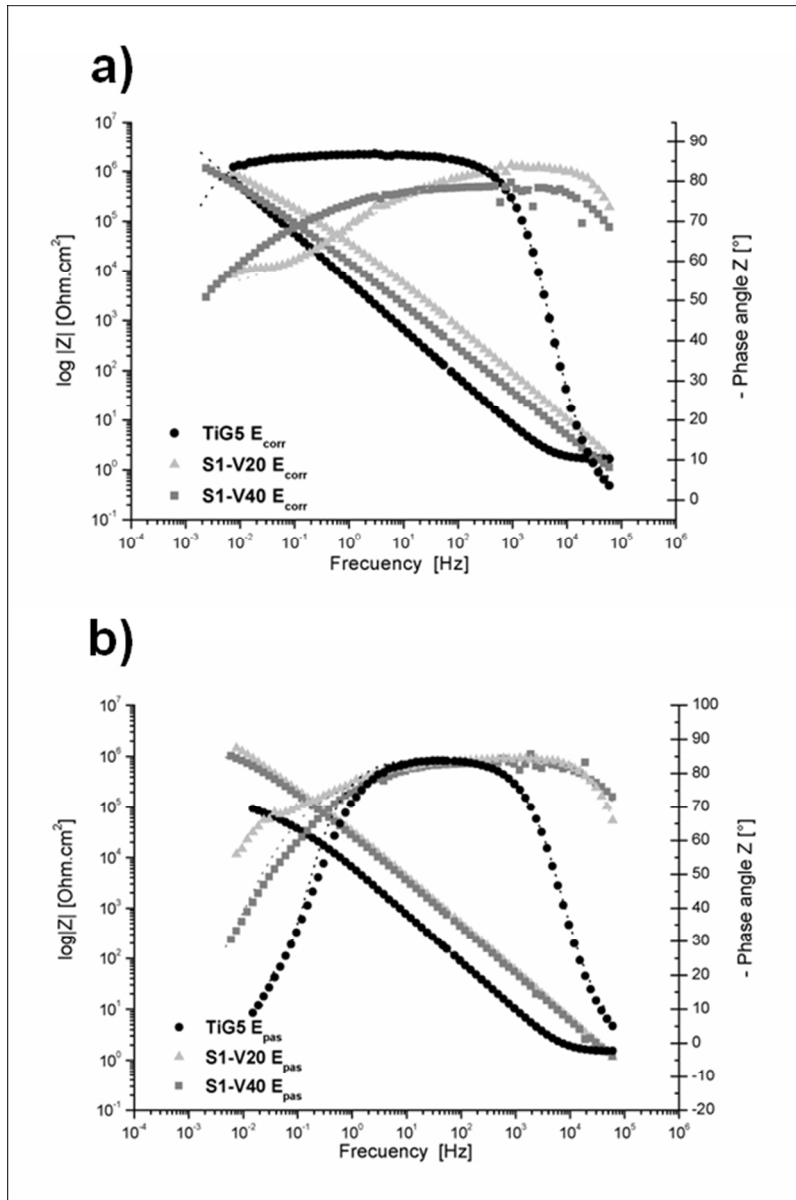
Figure 6. Bode diagrams of EIS results performed in 1 M sulphuric acid at: a) E_{corr}; b) passive potential of 0.6 mV$_{SCE}$.
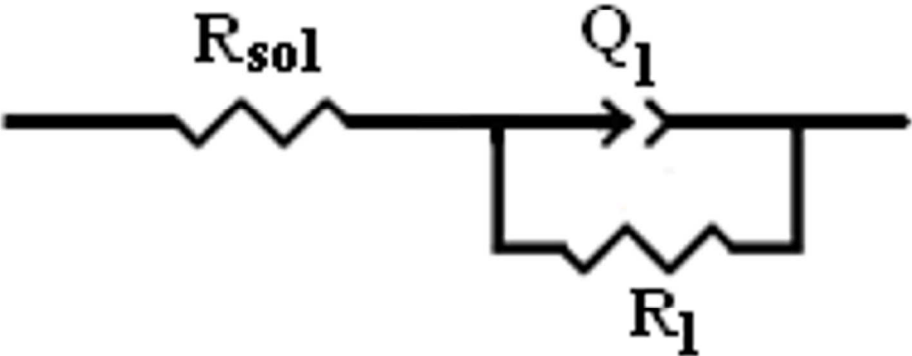100x150mm (150 x 150 DPI)

Figure 7. Randles circuit proposed to adjust EIS results of TiG5 sample at E_{corr} and E_{pas} in 1 M sulphuric acid of Figure 6 (a) and (b).
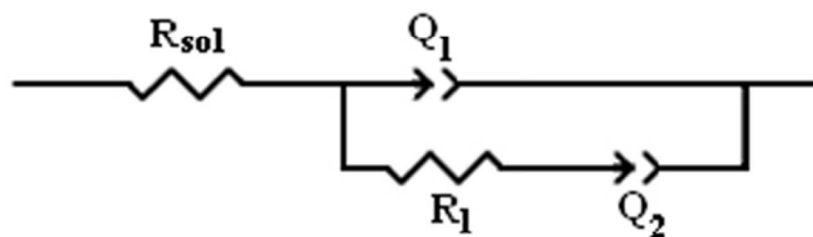
Figure 8. Equivalent circuit proposed to adjust EIS results of S1-V20 in 1 M sulphuric acid at E_{corr} of Figure 6 (a).

1
2
3
4
5
6
7
8
9
10
11
12
13
14
15
16
17
18
19
20
21
22
23
24
25
26
27
28
29
30
31
32
33
34
35
36
37
38
39
40
41
42
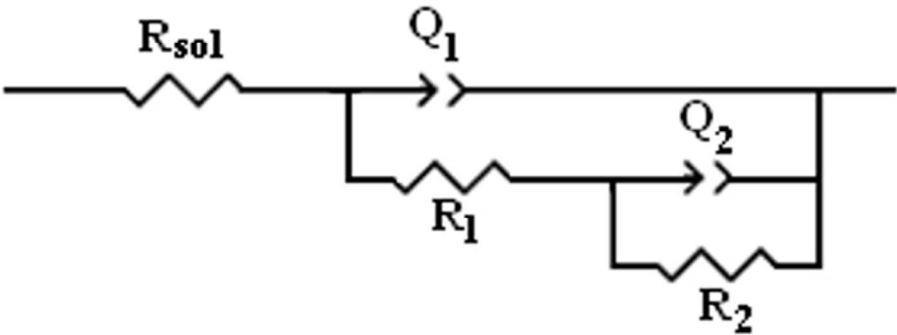43
44
45
46
47
48
49
50
51
52
53
54
55
56
57
58
59
60

Figure 9. Equivalent circuit proposed to adjust EIS results of S1-V40 in 1 M sulphuric acid at E_{corr} of Figure 6 (a).
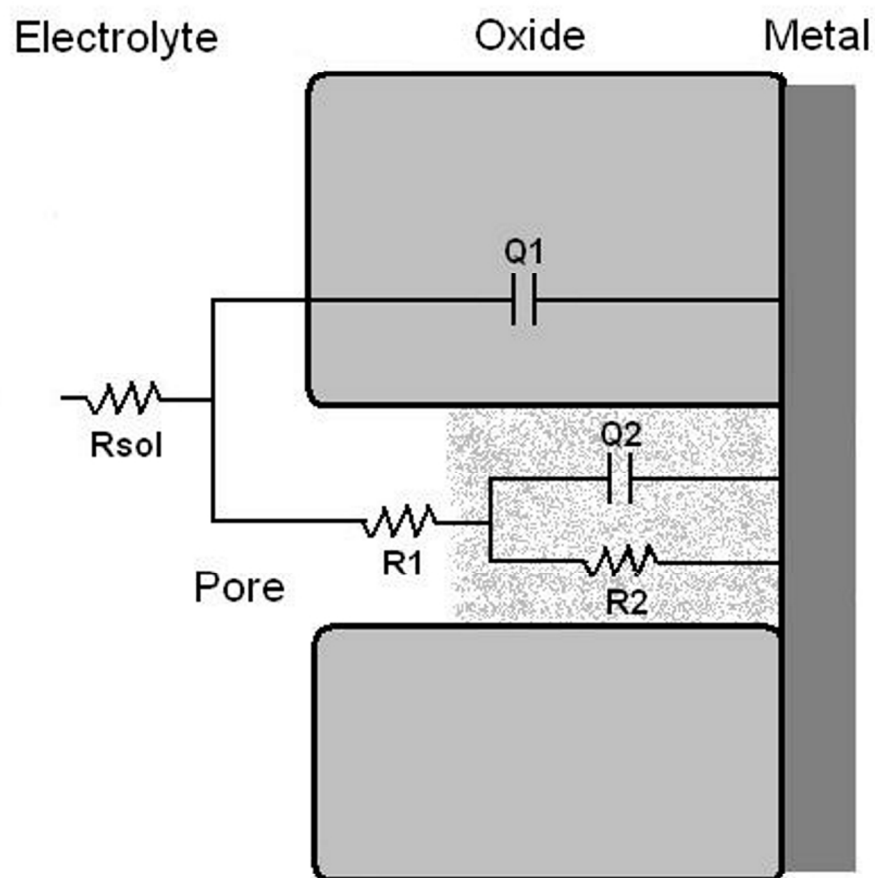
Figure 10. Schematic description of equivalent circuit proposed to adjust EIS results of S1-V40 in 1 M sulphuric acid at E_{corr} of Figure 6 (a). Adapted from [37].
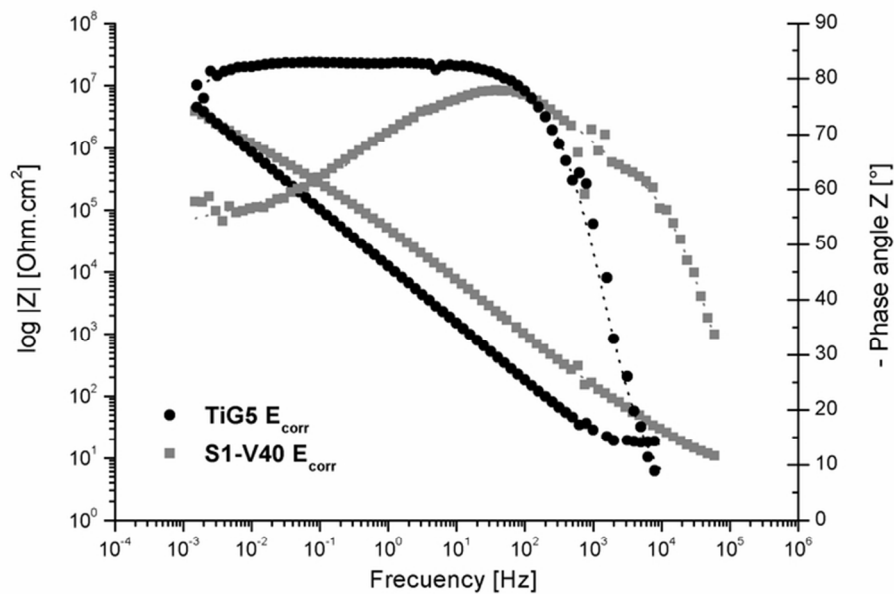
Figure 11. Bode diagram of EIS results performed in 0.9% sodium chloride at E_{corr}. 69x48mm (300 x 300 DPI)
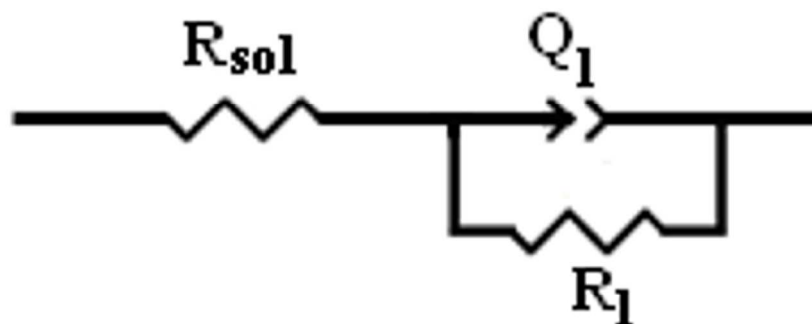
Figure 12. Randles circuit proposed to adjust EIS results of TiG5 sample in 0.9% sodium chloride at E_{corr} of Figure 11.
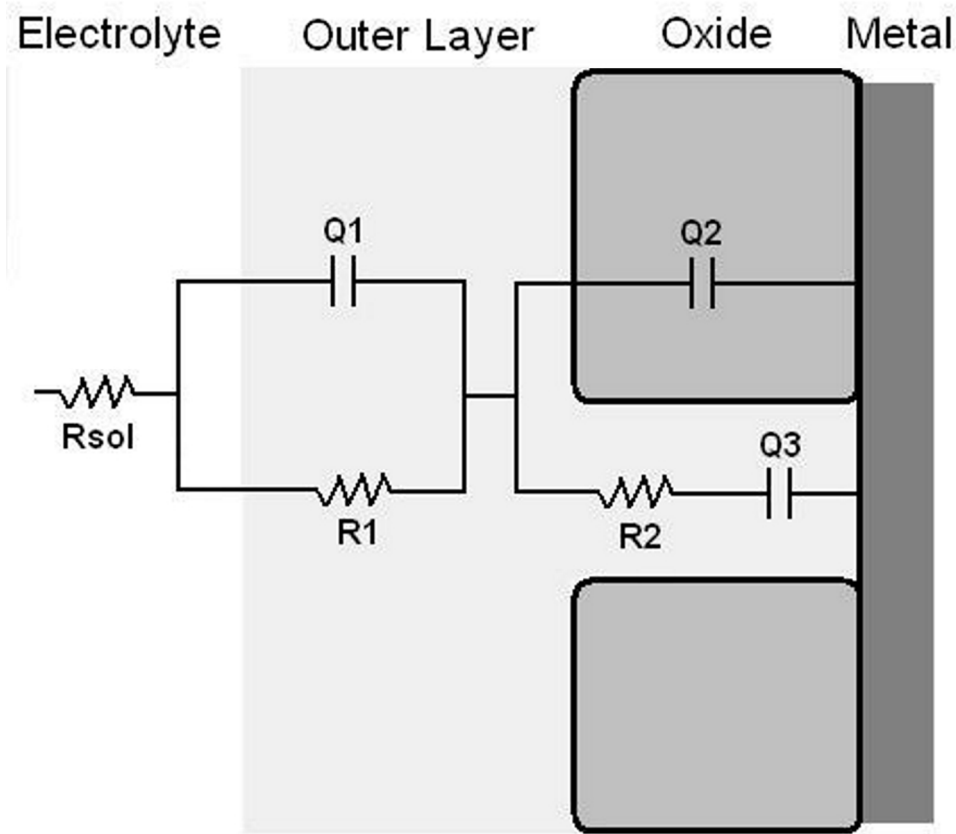
Figure 13. Equivalent circuit proposed to adjust EIS results of S1-V40 in 0.9% sodium chloride at E_{corr} of Figure 11.
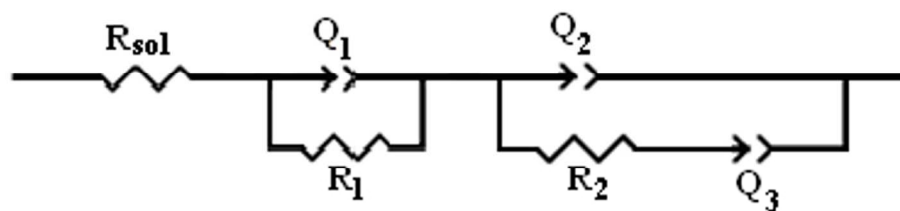
Figure 14. Schematic description of equivalent circuit proposed to adjust EIS results of S1-V40 in 0.9% sodium chloride at E_{corr} of Figure 11. Adapted from [37].

Tables

Table 1. Nomenclature, oxidation conditions, thickness and structure of the samples.

Group	Sample	Anodic oxidation [V]	Thermal treatment	Thickness [nm]	Structure[a]
	TiG5	no	no	-	α/β
A (pre-spark)	S1-V10	10	no	27	amorphous
	S1-V20	20	no	48	amorphous
	S1-V30	30	no	70	amorphous
	S1-V40	40	no	92	amorphous
	S1-V50	50	no	112	amorphous
	S1-V60	60	no	120 and 144	amorphous
A (post-spark)	S1-V70	70	no	> 168	a
	S1-V100	100	no	> 240	a + r
T	Ai-T500-t1	no	500 °C, 1h	20	amorphous
AT500	S1-V20-T500	20	500 °C, 1h	48	a + r
	S1-V40-T500	40	500 °C, 1h	100	a + r
	S1-V60-T500	60	500 °C, 1h	~ 120 and 144	a + r

[a] Structure column, the letters indicate the presence of phases: a = anatase; r = rutile; a + r = anatase and rutile.

Table 2. Electrochemical parameters extracted from the polarization curves of Figure 1.

Group	Sample	E_{corr} [mV$_{SCE}$]	i_{pas} [nAcm^{-2}]	E_{pas} [mV$_{SCE}$]	E_{pas}-E_{corr} [mV$_{SCE}$]	E_{trans} [mV$_{SCE}$]	E_{trans}-E_{pas} [mV$_{SCE}$]
	TiG5	-263	880	500	763	-[a]	-
A (pre-spark)	S1-V10	58	4	58	0	917	858
	S1-V20	150	5	150	0	620	470
	S1-V30	74	6	74	0	680	606
	S1-V40	198	4	198	0	620	422
	S1-V50	132	10	132	0	960	827
	S1-V60	156	5	156	0	960	804
A (post-spark)	S1-V70	102	5	102	0	650	547
	S1-V100	37	105	37	0	-*₁	-

[a] Remains passive, does not return to increase the current density in the range of potentials measured.

Table 3. Electrochemical parameters extracted from the polarization curves of Figure 4.

Group	Sample	E_{corr} [mV]	i_{pas} [nAcm^{-2}]	E_{pas} [mV]	$E_{pas}-E_{corr}$ [mV]	E_{trans} [mV]	$E_{trans}-E_{pas}$ [mV]
	TiG5	-263	880	500	763	-[a]	-
A (pre-spark)	**S1-V20**	150	5	150	0	620	470
	S1-V40	198	4	198	0	620	422
	S1-V60	156	5	156	0	960	804
T	**Ai-T500-t1**	-205	73	-[b]	-	-	-
AT500	**S1-V20-T500**	-214	74	-214	0	650	864
	S1-V40-T500	-112	35	-112	0	275	387
	S1-V60-T500	-130	75	-130	0	730	850

[a] Remains passive, does not again increase the current density in the range of potentials measured.

[b] The current is not stabilized in the range of potentials measured.

Table 4. Setting parameters of the equivalent circuit, EIS results in 1M sulphuric acid.

	Equivalent circuit	R_{sol} [$\Omega.cm^2$]	Q_1 [F/cm^2]	n_1	R_1 [$\Omega.cm^2$]	Q_2 [F/cm^2]	n_2	R_2 [$\Omega.cm^2$]
TiG5 E_{corr}	Figure 7	1.61	$2.85.10^{-5}$	0.96	$1.10.10^7$	-	-	-
S1-V20 E_{corr}	Figure 8	0.38	$2.65.10^{-6}$	0.95	$4.09.10^2$	$5.27.10^{-6}$	0.56	-
S1-V40 E_{corr}	Figure 9	0.21	$1.18.10^{-5}$	0.88	$1.13.10^{-14}$	$4.22.10^{-6}$	0.48	$1.28.10^7$
TiG5 E_{pas}	Figure 7	1.48	$2.66.10^{-5}$	0.94	$4.45.10^4$	-	-	-
S1-V20 E_{pas}	Figure 8	0.42	$3.65.10^{-6}$	0.97	$3.94.10^2$	$3.29.10^{-6}$	0.64	-
S1-V40 E_{pas}	Figure 9	0.25	$5.07.10^{-6}$	0.94	$1.14.10^{-14}$	$3.03.10^{-6}$	0.59	$1.6.10^6$

Table 5. Setting parameters of the equivalent circuits to the results of EIS in 0.9 % sodium chloride at E_{corr} .

	Equivalent circuit	R_{sol} [$\Omega.cm^2$]	Q_1 [F/cm^2]	n_1	R_1 [$\Omega.cm^2$]	R_2 [$\Omega.cm^2$]	Q_2 [F/cm^2]	n_2	Q_3 [F/cm^2]	n_3
TiG5 E_{corr}	Figure 12	1.61	$1.47.10^{-5}$	0.92	$5.71.10^7$	-	-	-		-
S1-V40 E_{corr}	Figure 13	1.06	$2.56.10^{-5}$	0.75	$3.20.10^1$	$1.87.10^5$	$3.56.10^{-6}$	0.88	$2.72.10^{-6}$	0.55